Stochastic Analysis of Sea Surface Wind Vectors: The Role of Multiplicative Noise

Philip Sura and Prashant D. Sardeshmukh

NOAA-CIRES Climate Diagnostics Center, Boulder, Colorado

September 9, 2004

Submitted to *JAS*

Corresponding author address:
Philip Sura
NOAA-CIRES Climate Diagnostics Center, R/CDC1
325 Broadway, Boulder, CO 80305-3328
Phone: (303) 497-4426, Fax: (303) 497-6449
E-Mail: Philip.Sura@noaa.gov

Abstract

Sea surface winds are known to be non-Gaussian almost everywhere on the globe, yet the detailed physical origin of the non-Gaussianity is not well established. This paper discusses the important role of state-dependent (that is, multiplicative) noise to account for non-Gaussian statistics. First, it is shown from data that the non-Gaussianity of midlatitude sea surface winds can not solely be described by non-linearities of effective deterministic dynamics; deviations from Gaussianity are rather due to multiplicative noise. Second, a simple model reveals that stochastically perturbing the drag coefficient of the momentum equations for a turbulent boundary layer is consistent with data. Perturbing the drag coefficient is, therefore, a physically consistent approach to stochastically parameterize subgrid scale processes.

1 Introduction

Stochastic differential equations (SDEs) offer a useful formalism for describing the nonlinear dynamics of the atmosphere and ocean over a wide range of time and spatial scales. The general idea of *stochastic climate models* was introduced by Hasselmann (1976) and is based on the Brownian motion analog: the observed red spectrum of oceanic fluctuations is a consequence of the amplification of low-frequency weather fluctuations. Stochastic models have been successful in describing atmospheric and oceanic variability within a broad frequency band (see e.g., Imkeller and von Storch 2001; Penland 2003a,b).

In stochastic atmospheric and oceanic models noise is introduced primarily as an additive process, where the strength of the noise is held constant and does not depend on the state of the system. However, the stochastic terms may also appear as multiplicative (that is, state-dependent) noise. Multiplicative noise is often identified with state-dependent variations of stochastic feedbacks from unresolved system components, and may be treated as stochastic perturbations of system parameters. The concept of multiplicative noise has various applications in fluid dynamics and, therefore, in the atmospheric/oceanic sciences. The importance of multiplicative noise to describe small-scale turbulence has been shown by Friedrich and Peinke (1997a,b) and Renner et al. (2001). Sura (2003) has recently shown that the accurate stochastic description of univariate midlatitude sea surface winds requires multiplicative noise. The potentially significant role of multiplicative noise to improve the representation of subgrid-scale phenomena in models of the climate systems has been stressed in several studies (e.g., Buizza et al. 1999; Palmer 2001; Sardeshmukh et al. 2001; Pérez-Muñuzuri et al. 2003; Sura 2002; Sura et al. 2004).

Sura et al. (2004) outlined a stochastic perspective on atmospheric regime behavior (or non-Gaussianity) based on a treatment of climate variability as a stochastic system with state-dependent noise. They demonstrated how some simple linear (or nearly linear) systems with multiplicative noise can produce non-Gaussian regime-like behavior without any intrinsic multimodality. The mere presence of non-Gaussianity, therefore, does not always imply that a system has deterministic nonlinear multiple regimes, nor that these regimes have a noticeable enhancement of persistence or predictability due to this nonlinearity. That apparently similar regimes can be induced by either slow or fast nonlinearities is illustrated in Fig. 1 [a more detailed discussion is given in Sura et al. (2004)].

In this paper the role of multiplicative noise to account for the observed non-Gaussianity of sea surface vector winds is studied. It is, therefore, an extension of Sura (2003) to two dimensions using techniques and theories discussed in Sura et al. (2004) (and Monahan 2004). Detailed knowledge of sea surface winds is, for example, vital to better understand and, in particular, to model wind-driven ocean variability (see e.g., Sura and Penland 2002; Sura and Gille 2003).

In Sura (2003) the need for a state-dependent noise term is interpreted by the observational fact that the variability (gustiness) of midlatitude winds increases with increasing wind speed; the multiplicative noise is then responsible for the non-Gaussianity of the winds. In Monahan (2004) another interpretation is given. He attributes the non-Gaussianity of the sea surface winds to the nonlinear surface drag predicted for a turbulent boundary layer by Monin-Obukhov similarity theory. Nevertheless, the univariate results in Sura (2003) are broadly consistent with the white-noise limit of the simple stochastic boundary layer model

developed in Monahan (2004): in his white-noise limit the stochastic terms appear as multiplicative noise. Yet, Monahan (2004) claims that the non-Gaussianity of the winds is due to the nonlinear surface drag.

In this paper it is exemplary shown for the Southern Ocean that a bivariate stochastic description of sea surface vector winds requires multiplicative noise. In particular, the non-Gaussianity of the winds can not solely be accounted for by non-linearities of the effective deterministic dynamics. First, in section 2, some principal ideas of stochastic dynamics are briefly reviewed. The data are described in section 3, and results are presented in section 4. Finally, section 5 provides a summary and a discussion.

2 Stochastic Dynamics in a Nutshell

This section introduces a few basic ideas of stochastic dynamics used in this paper. More comprehensive treatises can be found in many textbooks (e.g., Gardiner 1985; Horsthemke and Léfever 1984; Paul and Baschnagel 1999).

Consider the dynamics of an n-dimensional system whose state vector $\mathbf{x}$ is governed by the SDE

$$\frac{d\mathbf{x}}{dt} = \mathbf{A}(\mathbf{x}) + \mathbf{B}(\mathbf{x})\boldsymbol{\eta} \ , \tag{1}$$

where the vector $\mathbf{A}$ represents all slow processes and $\mathbf{B}(\mathbf{x})\boldsymbol{\eta}$, with the matrix $\mathbf{B}$ and the noise vector $\boldsymbol{\eta}$, represents the stochastic approximation to the fast nonlinear processes. The

stochastic components η_i are assumed to be independent Gaussian white-noise processes:

$$\langle \eta_i(t) \rangle = 0, \qquad \langle \eta_i(t) \eta_i(t') \rangle = \delta(t - t') \ , \tag{2}$$

where $\langle ... \rangle$ denotes the averaging operator. The corresponding Fokker-Planck equation,

$$\begin{aligned} \frac{\partial p(\mathbf{x}, t)}{\partial t} = & - \sum_i \frac{\partial}{\partial x_i} \left[A_i + \alpha \sum_{j,k} \left(\frac{\partial}{\partial x_j} B_{ik} \right) B_{jk} \right] p(\mathbf{x}, t) \\ & + \frac{1}{2} \sum_{i,j} \frac{\partial^2}{\partial x_i \partial x_j} (\mathbf{B}\mathbf{B}^T)_{ij} p(\mathbf{x}, t) \ , \end{aligned} \tag{3}$$

describes the conservation of the probability density $p(\mathbf{x}, t)$ of the system described by the SDE (1). Two different values of α yield two physically important stochastic calculi: the Itô ($\alpha = 0$) and the Stratonovich calculus ($\alpha = 1/2$). On the right hand side, the first term within square brackets describes the dynamics of the deterministic system and is called the deterministic drift. The second term within square brackets, which does not occur in Itô systems ($\alpha = 0$), is called the noise-induced drift. The remaining term is associated with the diffusion of the probability density by noise.

For a detailed discussion of stochastic integration and the differences between Itô and Stratonovich SDEs see for example Horsthemke and Léfèver (1984), Gardiner (1985), or Penland (1996). The key point here is that the Stratonovich calculus is relevant for continuous physical systems, such as the atmosphere, in which rapidly fluctuating quantities with small but finite correlation times are approximated as white-noise. Thus, simplified stochastic models constructed from atmospheric dynamical equations may assume Stratonovich calculus. However, if instead a stochastic model is indirectly estimated from observed discrete data, then the inferred drift will be the *sum* of the deterministic and the noise-induced drifts. In this case using the Itô framework may be preferable, where now $\mathbf{A}(\mathbf{x})$ represents not just

the deterministic drift but rather this sum, or the "effective drift".

Equations for moments of $\mathbf{x}$ can be obtained by multiplying the Fokker-Planck equation (3) by polynomials and integrating over the domain of the systems. In particular, seconds moments of $\mathbf{x}$ are given by

$$\frac{\partial \langle \mathbf{x}\, \mathbf{x}^T \rangle}{\partial t} = \langle \mathbf{A}(\mathbf{x})\, \mathbf{x}^T \rangle + \langle \mathbf{x}\, \mathbf{A}(\mathbf{x})^T \rangle + \langle \mathbf{B}(\mathbf{x})\, \mathbf{B}(\mathbf{x})^T \rangle \,. \tag{4}$$

This equation is known as the fluctuation-dissipation relation (FDR) of the system (see e.g., Penland 1996). The FDR relates the variance of the stochastic fluctuations to the magnitude of the dissipation.

In principle, the effective deterministic and stochastic parts of (3) can be determined from data by using their statistical definitions (Siegert et al. 1998; Friedrich et al. 2000; Gradišek et al. 2000; Sura and Barsugli 2002; Sura 2003; Sura and Gille 2003):

$$\mathbf{A}(\mathbf{x}) = \lim_{\Delta t \to 0} \frac{1}{\Delta t} \langle \mathbf{X}(t + \Delta t) - \mathbf{x} \rangle |_{\mathbf{X}(t)=\mathbf{x}} \quad , \tag{5}$$

$$\mathbf{B}(\mathbf{x})\mathbf{B}^T(\mathbf{x}) = \lim_{\Delta t \to 0} \frac{1}{\Delta t} \langle (\mathbf{X}(t + \Delta t) - \mathbf{x})(\mathbf{X}(t + \Delta t) - \mathbf{x})^T \rangle |_{\mathbf{X}(t)=\mathbf{x}} \quad , \tag{6}$$

where $\mathbf{X}(t + \Delta t)$ is a solution (a single stochastic realization) of the SDE (1) with the initial condition $\mathbf{X}(t) = \mathbf{x}$ at time t. The data define a state space representing every observed value of $\mathbf{x}$. The effective drift and stochastic diffusion are estimated by replacing the theoretical limit $\Delta t \to 0$ with a finite-difference approximation. In practice, estimating $\mathbf{A}(\mathbf{x})$ and $\mathbf{B}(\mathbf{x})\mathbf{B}^T(\mathbf{x})$ from discretely sampled data is prone to error, because Taylor expansions of stochastic terms are proportional to $\sqrt{\Delta t}$ and not proportional to Δt as are the deterministic terms (e.g., Sura and Barsugli 2002; Sura 2003; Ragwitz and Kantz 2001; Friedrich et al. 2002).

3 Data

In this study observed global 6-hourly ocean surface winds are used. The data are derived from a space and time blending of QuikSCAT scatterometer observations and NCEP reanalyses (Chin et al. 1998; Milliff et al. 1999). The blending method creates global fields by retaining QuikSCAT wind retrievals in swath regions, and in the unsampled regions augmenting the low-wavenumber NCEP fields with a high-wavenumber component that is derived from monthly regional QuikSCAT statistics. 6-hourly maps of 10 m zonal (u) and meridional (v) wind components are available at a resolution of $0.5^\circ \times 0.5^\circ$ from 88°S to 88°N. The data used cover the period July 20, 1999 to December 31, 2003. The data files are available from the National Center for Atmospheric Research (NCAR) Data Support Section (DSS) at the URL **http://dss.ucar.edu/datasets/ds744.4/**. A detailed description of the blended wind product similar to the one used in the present paper can be found in Milliff et al. (1999), and the details of the blending method are described in Chin et al. (1998). Statistical properties and of the QuikSCAT surface wind were recently analyzed by Patoux and Brown (2001) and Gille (2003).

In reanalyzed datasets (NCEP or ECMWF) observations are assimilated within an atmospheric model to produce the analyzed fields that are consistent with the model dynamics. Nevertheless, the spatial and temporal coverage of observations over the oceans (in particular over the Southern Ocean) is very limited. That is, the used QuikSCAT based dataset contains much more wind observations over the oceans than the reanalyzed products. Therefore, in contrast to NCEP or ECMWF data, the QuikSCAT based wind data over the oceans are regarded as observations, not as model output. Indeed, scatterometer winds are shown

to be tremendously accurate (Bourassa et al. 1997) and are expected to be more reliable than reanalyzed datasets (Patoux and Brown 2001). Nonetheless, the disadvantage of the QuikSCAT dataset is that it covers a rather short period.

Because an accurate estimation of the effective drift $\mathbf{A}(\mathbf{x})$ and the diffusion $\mathbf{B}(\mathbf{x})\mathbf{B}^T(\mathbf{x})$ requires long time series, in particular for the bivariate case, it is not possible to obtain reliable estimates at each grid-point. 53 months of 6-hourly wind fields yield 6452 data points in time, which is insufficient to obtain robust high-quality estimates of $\mathbf{A}(\mathbf{x})$ and $\mathbf{B}(\mathbf{x})\mathbf{B}^T(\mathbf{x})$ for the bivariate wind vectors. To circumvent this problem, artificial "time series", which retain the stochastic properties of the wind fields as a function of latitude, can be constructed in the following way. Estimates of spatial autocorrelations for Southern Ocean QuikSCAT winds indicate decorrelation scales of about 1000 km in the zonal direction and 1500 km in the meridional direction (not shown). A comparable zonal spatial decorrelation scale is valid for the midlatitude Atlantic and Pacific storm tracks. For tropical and subtropical regions the zonal spatial decorrelation scale is smaller, because there the atmospheric variability is dominated by relatively small scale convective events.

Therefore, grid-points that are separated by 1000 km or more in the zonal direction can be treated as stochastically independent locations representing independent realizations of the same stochastic process. The zonal dependence, as well as the annual cycle, of the wind field are neglected by normalizing the time series to have zero mean and unit standard deviation. This is done by normalizing the data for each month and every chosen zonal location. Finally, several 53 months long time series can be concatenated to obtain a longer "time series" which retains the overall stochastic dynamical properties of the actual wind

field as a function of latitude. The resulting time series can be interpreted as normalized zonally averaged wind speeds.

Here, this procedure is carried out for the Southern Ocean, which yields 20 locations in longitude. Then the concatenated dataset has 129040 records, which turns out to be sufficient to obtain robust high-quality estimates of $\mathbf{A}(\mathbf{x})$ and $\mathbf{B}(\mathbf{x})\mathbf{B}^T(\mathbf{x})$ for the bivariate wind vectors.

4 Results

In section 4.1 the univariate case for the Southern Ocean already discussed in Sura (2003) is briefly revisited with updated QuikSCAT data in order to introduce the basic concepts of multiplicative noise in sea surface winds. In section 4.2 the stochastic analysis is extended to bivariate vector winds and compared to results from a simple stochastic boundary layer model presented in Monahan (2004). Because it is already known that the basic stochastic properties of midlatitude sea surface winds are nearly the same all over the globe (Sura 2003), this paper confines its analysis to the Southern Ocean as an exemplary case study for midlatitude winds.

4.1 The univariate case revisited

In the univariate case the governing SDE is

$$\frac{dx}{dt} = A(x) + B(x)\eta \;, \tag{7}$$

where x is the zonal wind velocity (u), and the meridional wind component (v) respectively. To evaluate $A(x)$ and $B(x)$ using the one-dimensional finite-difference versions of Eqs. (5) and (6), the interval spanned by the data is divided into 50 equal bins (sensitivity experiments with different numbers of bins were performed as well, but the general results discussed below did not change). In the following, the smallest possible discrete time step of 6 hours is used for Δt in the finite-difference approximation, except for an error estimation. Actually, the most practical way to detect the systematic error made by using a finite time step is to change Δt and to compare the results. Therefore, the use of different time steps Δt ensures that the systematic error made by using a finite-difference approximation of Eqs. (5) and (6) is small and neglectable [see Sura and Barsugli (2002) or Sura (2003) for a more detailed discussion].

Another important point to look at is if the white-noise assumption made in Eqs. 1 and 7 is actually valid for the data used. This can be done in a straightforward way. For any observation $x_{obs}(t)$ the effective drift $A(x)$ estimated from data (see below) can be used to calculate a 6-hourly time step Δt: $x(t+\Delta t) = A(x)\Delta t + x_{obs}(t)$. If the white-noise assumption is correct the difference between the observed value $x_{obs}(t+\Delta t)$ and the modeled value $x(t+\Delta t)$ should equal the non-Gaussian multiplicative white-noise term $B(x)\eta$. For the univariate winds relevant statistical properties of the residuals $r \equiv x_{obs}(t+\Delta t) - x(t+\Delta t)$ are discussed below.

As described in Sura (2003), the method yields stable results for 6-hourly midlatitude winds. That is, the finite-difference estimates of $A(x)$ and $B(x)$ do not depend sensitively on the time step Δt. The estimated functions $A(x)$ and $B(x)$ for the zonal and meridional

winds at 50°S are shown in Fig. 2. The dimensional zonally averaged zonal and meridional wind speeds are $\overline{u} = 6.6$ m s^{-1} and $\overline{v} = -1.1$ m s^{-1}. The corresponding zonally averaged standard deviations are $\overline{\sigma}_u = 5.6$ m s^{-1} and $\overline{\sigma}_v = 6.5$ m s^{-1}. Note that the normalized wind speeds, for example the zonal wind u, can be transformed into dimensional winds through the relation $x^* = x\,\overline{\sigma}_u + \overline{u}$, whereby x denotes normalized winds and x^* dimensional winds. Therefore, zero flow is attained for $x = -\overline{u}/\overline{\sigma}_u$.

Autocorrelation functions and PDFs of the residuals $r \equiv x_{obs}(t + \Delta t) - x(t + \Delta t)$ for the zonal and meridional winds are shown in Fig. 3. For both the zonal and the meridional wind the autocorrelation is close to zero after one time step of 0.25 days (Figs. 3a,b). That is, the residual is uncorrelated on the resolved time scale and the white-noise approximation is indeed justified. Moreover, the PDFs of the residuals are highly non-Gaussian (actually close to an exponential distribution), once again indicating that multiplicative white-noise is essential to describe the residual (Figs. 3c,d).

The general features in Fig. 2 were already discussed in Sura (2003). To recapitulate, for zonal and meridional winds the deterministic contribution $A(x)$ consists of a nearly linear damping term with a damping time scale of about 1 day. More importantly, a proper description of the winds requires a state-dependent white-noise term, that is, multiplicative noise. The method used reveals another remarkable characteristic of the underlying timeseries. The diffusion functions $B(x)$ are not symmetric with respect to the mean flow ($x = 0$), nor are they symmetric with respect to zero zonal ($x = -\overline{u}/\overline{\sigma}_u = -1.18$) or zero meridional flow ($x = -\overline{v}/\overline{\sigma}_v = 0.17$). In Sura (2003) the need for a state-dependent noise term is interpreted by the observational fact that the variability (gustiness) of midlatitude

winds increases with increasing wind speed. In Monahan (2004) another interpretation is given; he attributes the non-Gaussianity of the surface winds to the nonlinear surface drag predicted for a turbulent boundary layer by Monin-Obukhov similarity theory (see Eq. 12 below). The univariate results in Sura (2003) are broadly consistent with the white-noise limit of the simple stochastic boundary layer model developed in Monahan (2004): in his white-noise limit the stochastic terms appear as multiplicative noise.

The PDFs of the zonal and meridional winds are shown in Fig. 4. Note that the zonal wind is highly non-Gaussian, whereas the meridional wind is nearly Gaussian. This is in agreement with other studies of sea surface winds (e.g., Gille 2003; Monahan 2004).

It is important to note that, as shown above, the white-noise approximation is valid for the data used. Furthermore, it should be noted that the finite-difference estimates of $A(x)$ and $B(x)$ are accurate. In particular, the asymmetry of $B(x)$ is not an artifact of the estimation algorithm, as suggested by Monahan (2004). Systematic errors are ruled out in two different ways. One the one hand, the use of different time steps Δt ensures that the error made by using a finite-difference approximation is small and neglectable. On the other hand, by inserting the effective drift $A(x)$, the state-dependent diffusion $B(x)$, and the PDF (Fig. 4) of the data into the steady state Fokker-Planck equation, the probability budget has to be balanced if $A(x)$ and $B(x)$ ought to be correct. It turns out the Fokker-Planck equation is indeed balanced, and, therefore, the estimates of $A(x)$ and $B(x)$ are correct. Furthermore, due to the length of the record, sampling errors are very small and neglectable.

4.2 The bivariate case

The joint PDF of the normalized zonal (u) and meridional wind (v), determined by dividing the interval $[-4:4,-4:4]$ into 20×20 equal bins is shown in Fig. 5a (sensitivity experiments with different numbers of bins were performed as well, but the general structure of the PDF did not change). Positive (negative) departures from Gaussianity (Fig. 5b) indicate that the observed PDF is greater (smaller) than the corresponding bivariate Gaussian distribution. The departures from Gaussianity are statistically significant at the 95% confidence level determined using a Monte-Carlo method (e.g., Kimoto and Ghil 1993). Note that the joint PDF is highly non-Gaussian in the x-direction (zonal wind) and nearly Gaussian in the y-direction (meridional wind), in agreement with the marginal PDFs in Fig. 4.

4.2.1 Balancing the probability budget

Using the Fokker-Planck equation (3), a steady probability budget for the vector winds ($i=1,2;j=1,2$) can be written as

$$-\sum_i \frac{\partial}{\partial x_i} A_i p(\mathbf{x},t) + \frac{1}{2}\sum_{i,j} \frac{\partial^2}{\partial x_i \partial x_j} (\mathbf{B}\mathbf{B}^T)_{ij} p(\mathbf{x},t) = 0 \ . \tag{8}$$

That is, in a time-averaged sense, the effective drift balances the stochastic diffusion. One can then ask whether the eventually nonlinear effective drift, estimated by using its finite-difference approximation (5), is sufficient to produce the non-Gaussianity of the observed PDF. Thus, it is asked whether or not the probability budget can be balanced using purely additive stochastic forcing.

The effective drift of the data components is shown in Fig. 6. Because of the long dataset

the statistical uncertainties are very small (not shown): the standard error is smaller than 0.2 for most of the points.

At this point it is, again, important to test if the white-noise assumption made in the bivariate version of Eqs. 1 is actually valid for the data used. For any observation $\mathbf{x}_{obs}(t)$ the effective drift $\mathbf{A}(\mathbf{x})$ estimated from data (see Fig. 6) can be used to calculate a 6 hourly time step Δt: $\mathbf{x}(t+\Delta t) = \mathbf{A}(\mathbf{x})\Delta t + \mathbf{x}_{obs}(t)$. If the white-noise assumption is correct the residual $\mathbf{r} \equiv \mathbf{x}_{obs}(t+\Delta t) - \mathbf{x}(t+\Delta t)$ should equal the non-Gaussian multiplicative white-noise term $\mathbf{B}(\mathbf{x})\boldsymbol{\eta}$. Autocorrelation functions and PDFs of the residual are shown in Fig. 7. As for the univariate winds, the autocorrelations are close to zero after one time step of 0.25 days (Figs. 7a,b). That is, the residual is uncorrelated on the resolved time scale and the white-noise approximation is indeed justified. Moreover, the PDFs of the residual are highly non-Gaussian (actually close to an exponential distribution), indicating that multiplicative white-noise is essential to describe the residual (Figs. 7c,d).

Now, as we know that the white-noise approximation is valid, we are in the position to ask whether or not the probability budget can be balanced using pure additive white-noise. Because the direct estimation of the diffusion term is prone to large systematic errors (Sura and Barsugli 2002), a different tack is used to see whether additive noise can balance the probability budget. First, Eq. (8) is rewritten for the special case where $\mathbf{B}$ is purely additive ($i = 1, 2; j = 1, 2$):

$$-\sum_i \frac{\partial}{\partial x_i} A_i p(\mathbf{x}, t) + \frac{1}{2} \sum_{i,j} (\mathbf{B}_A \mathbf{B}_A^T)_{ij} \frac{\partial^2}{\partial x_i \partial x_j} p(\mathbf{x}, t) = R \ . \tag{9}$$

Given the effective drift $\mathbf{A}(\mathbf{x})$ (Fig. 6), the steady-state FDR (4) can be used to determine

the corresponding additive noise matrix $\mathbf{B}_A\mathbf{B}_A^T$:

$$\mathbf{B}_A\mathbf{B}_A^T = \begin{pmatrix} 1.834 & 0.434 \\ 0.434 & 2.146 \end{pmatrix} \quad . \tag{10}$$

Using the PDF (Fig. 5), the effective drift (Fig. 6), and pure additive noise given by the matrix (10), the two terms on the left hand side of the Fokker-Planck equation (9) are evaluated and shown in Figs. 8a and 8b. The sum (the residual R) (significant at the 95% confidence level, determined using a Monte-Carlo method) of both terms is shown in Fig. 8c. The residual is not zero, indicating that pure additive noise is not able to balance the probability budget.

If we partition the net noise effect $\mathbf{B}\mathbf{B}^T$ in (8) into an additive noise term $\mathbf{B}_A\mathbf{B}_A^T$ and a multiplicative noise term $\mathbf{B}_R\mathbf{B}_R^T$, then $-R$ would represent the multiplicative part:

$$R = -\frac{1}{2}\sum_{i,j}\frac{\partial^2}{\partial x_i \partial x_j}\left(\mathbf{B}_R\mathbf{B}_R^T\right)_{ij} p(\mathbf{x},t) \quad , \tag{11}$$

with R and $\mathbf{B}_A\mathbf{B}_A^T$ appropriately scaled so that the corresponding Fluctuation-Dissipation relation is satisfied.

In summarizing, if the departures from Gaussianity are primarily due to the nonlinear effective drift term, then the probability budget for the joint PDF would be balanced with pure additive noise. Clearly, it is not; all three terms of the Fokker-Planck equation have the same order of magnitude. Positive (negative) values mean that the additive noise is too weak (strong) to balance the drift. Thus, the observed departures from Gaussianity result not solely from the nonlinear drift term but rather from the multiplicative structure of the noise.

Recognize that the deviations from Gaussianity in Fig. 5b and the multiplicative noise contribution ($-R$) in Fig. 8c are broadly consistent with the schematic sketch in Fig. 1. The positive deviation from Gaussianity happens to be due to relatively weak noise, whereas the negative deviations are due to relatively strong noise.

4.2.2 Direct noise estimation and stochastic boundary layer dynamics

It has been shown in the previous section that multiplicative noise is vital to balance the probability budget of the sea surface winds. That is, the non-Gaussianity of the joint wind PDF is basically due to multiplicative noise, and not to the effective deterministic drift. In this section we estimate the state-dependent noise matrix directly from data, and compare the results to a simple stochastic model derived in Monahan (2004).

In general, estimating the multiplicative noise matrix $\mathbf{B}(\mathbf{x})\mathbf{B}^T(\mathbf{x})$ from discretely sampled data is prone to error (Sura and Barsugli 2002; Sura 2003). Nevertheless, it has been shown in Sura (2003) that an accurate univariate estimation of the noise term is possible for the dataset used. Thus, we use Eq. 6 to estimate the matrix $\mathbf{B}(\mathbf{x})\mathbf{B}^T(\mathbf{x})$, keeping in mind that the results should be checked very carefully.

In the following, the smallest possible discrete time step of 6 hours is used for Δt in the finite-difference approximation, except for an error estimation. As already mentioned in section 4.1, the most practical way to detect the systematic error made by using a finite time step is to change Δt and to compare the results. Here the method yields stable results. That is, the finite-difference estimate of $\mathbf{B}(\mathbf{x})\mathbf{B}^T(\mathbf{x})$ does not depend sensitively on the time step Δt. In particular, the results are the same for time steps of $\Delta t = 6, 12$, and 18 h. That

is, the error terms proportional to Δt are small and neglectable for those time steps. The estimates diverge for time steps equal to or larger than 24 h.

The elements of the matrix $\mathbf{B}(\mathbf{x})\mathbf{B}^T(\mathbf{x})$ are shown in Fig. 9. Because of the long dataset the statistical uncertainties are very small (not shown): the standard error is smaller than 0.4 for most of the points. $(\mathbf{B}\mathbf{B}^T)_{11}$ is basically a function of x, and increases for increasing absolute values $|x|$. The minimum is approximately at $x = 0$. Note that, however, $(\mathbf{B}\mathbf{B}^T)_{11}$ is not symmetric with respect to the line $x = 0$; the downslope gradient of $(\mathbf{B}\mathbf{B}^T)_{11}$ is larger for negative x than it is for positive x. $(\mathbf{B}\mathbf{B}^T)_{22}$ is basically a function of y, and increases for increasing absolute values $|y|$. The minimum is approximately at $y = 0$. Again, note that $(\mathbf{B}\mathbf{B}^T)_{22}$ is not symmetric with respect to the line $y = 0$; the downslope gradient of $(\mathbf{B}\mathbf{B}^T)_{22}$ is larger for negative y than it is for positive y. The off-diagonal element $(\mathbf{B}\mathbf{B}^T)_{12}$ (note that $\mathbf{B}\mathbf{B}^T$ is symmetric: $(\mathbf{B}\mathbf{B}^T)_{12} = (\mathbf{B}\mathbf{B}^T)_{21}$) is almost symmetric with respect to the origin of the coordinate system; in quadrant I $(\mathbf{B}\mathbf{B}^T)_{12}$ is positive, in quadrant II $(\mathbf{B}\mathbf{B}^T)_{12}$ is negative, and so forth. Nevertheless, the absolute gradients in each quadrant are slightly different.

Next the empirical results of the noise matrix $\mathbf{B}(\mathbf{x})\mathbf{B}^T(\mathbf{x})$ are compared to a simple stochastic boundary layer model, where the drag coefficient is perturbed stochastically (Monahan 2004). Suppose the surface drag $\boldsymbol{\tau}$ of the turbulent boundary layer is parameterized by a closure given by Monin-Obukhov similarity theory, as in Monahan (2004): $\boldsymbol{\tau} = C_D|\mathbf{u}|\mathbf{u}$, with the drag coefficient C_D. Then the linearized momentum equations for a boundary layer of thickness h may be written as

$$\frac{\partial u}{\partial t} = -\frac{1}{\rho}\frac{\partial p}{\partial x} + fv - \frac{C_D}{h}\sqrt{u^2+v^2}\,u \ ,$$

$$\frac{\partial v}{\partial t} \;=\; -\frac{1}{\rho}\frac{\partial p}{\partial y} - fu - \frac{C_D}{h}\sqrt{u^2+v^2}\,v \;\;, \tag{12}$$

where p denotes pressure, ρ density, and f the Coriolis parameter. The downward transport of momentum has been neglected for the sake of simplicity. A detailed discussion of boundary layer dynamics can be found in many textbooks (e.g., Haltiner and Williams 1980). In the following we consider stochastic fluctuations in the drag coefficient C_D. Thus, C_D stochastically fluctuates around the mean value $\overline{C}_D$: $C_D = \overline{C}_D + \eta^M(t)$. The fluctuations $\eta^M(t)$ are assumed to be Gaussian white-noise with zero mean and amplitude σ^M: $< \eta^M >= 0$, $< \eta^M(t)\,\eta^M(t') >= (\sigma^M)^2\delta(t-t')$. Because of the Gaussian distribution of the noise it is possible that $\overline{C}_D + \eta^M(t)$ becomes negative occasionally. Despite the fact that the deterministically defined mean drag coefficient cannot become negative, this is not a conceptual problem because it is known that turbulent eddy fluxes can occasionally change their sign as well. The corresponding SDE can be written in vector form (see Eq. 1), with $\mathbf{x} \equiv (u,v)^T$, where the effective drift $\mathbf{A}(\mathbf{x})$ reads

$$\mathbf{A}(\mathbf{x}) = \begin{pmatrix} \overline{\Pi}_u - \frac{\overline{C}_D}{h}\sqrt{u^2+v^2}\,u + (\frac{\sigma^M}{h})^2(u^2+v^2)u \\ \\ \overline{\Pi}_v - \frac{\overline{C}_D}{h}\sqrt{u^2+v^2}\,v + (\frac{\sigma^M}{h})^2(u^2+v^2)v \end{pmatrix} \;\;, \tag{13}$$

with the mean forcings $\overline{\Pi}_u = \overline{-\rho^{-1}\partial p/\partial x + fv}$, and $\overline{\Pi}_v = \overline{-\rho^{-1}\partial p/\partial y - fu}$ [see Monahan (2004) for a detailed discussion; however, note the inconsistency in Monahan's SDE for u and v because Π_u and Pi_v are itself functions of u and v]. For zero mean forcings ($\overline{\Pi}_u = \overline{\Pi}_v = 0$) and typical values of h, $\overline{C}_D$, and σ^M, the components of $\mathbf{A}(\mathbf{x})$ are shown in Fig. 10. Note the similarity with the drift directly estimated from data (Fig. 6); the differences are discussed

below. The matrix $\mathbf{B}(\mathbf{x})$ is

$$\mathbf{B}(\mathbf{x}) = \begin{pmatrix} \frac{\sigma^M}{h}\sqrt{u^2+v^2}\; u & 0 \\ \frac{\sigma^M}{h}\sqrt{u^2+v^2}\; v & 0 \end{pmatrix} \quad , \tag{14}$$

and the normalized noise vector is $\boldsymbol{\eta} = (\eta^M/\sigma^M, 0)^T$. Therefore, $\mathbf{B}(\mathbf{x})\mathbf{B}^T(\mathbf{x})$ becomes

$$\mathbf{B}(\mathbf{x})\mathbf{B}^T(\mathbf{x}) = \begin{pmatrix} (\frac{\sigma^M}{h}\sqrt{u^2+v^2}\; u)^2 & (\frac{\sigma^M}{h}\sqrt{u^2+v^2})^2\; uv \\ (\frac{\sigma^M}{h}\sqrt{u^2+v^2})^2\; uv & (\frac{\sigma^M}{h}\sqrt{u^2+v^2}\; v)^2 \end{pmatrix} \quad . \tag{15}$$

The theoretically derived elements of the matrix $\mathbf{B}(\mathbf{x})\mathbf{B}^T(\mathbf{x})$ (scaled to have the same order of magnitude as the matrix estimated from normalized wind data) are shown in Fig. 11. Note the general similarity with the matrix directly estimated from data (Fig. 9). That means, stochastically perturbing the drag coefficient of the momentum equations for a turbulent boundary layer is approximately consistent with data.

Yet there are differences. The discrepancies may be a consequence of simplifying assumptions, for example the negligence of the downward momentum transport. Moreover, the normalization of the winds before estimating the drift and diffusion coefficients could lead to biases, as the drag is a function of the total wind speed and not its standardized anomaly. Nevertheless, while the agreement between $\mathbf{B}(\mathbf{x})\mathbf{B}^T(\mathbf{x})$ estimated from data (Fig. 9) and its theoretically derived counterpart (Fig. 11) is not perfect, the main qualitative features are captured by the simple white-noise model.

5 Summary and Discussion

This paper outlined the role of multiplicative noise in the stochastic description of sea surface wind vectors. It has been exemplary shown for the Southern Ocean that the observed departures from Gaussianity do not solely result from the effective drift, but from the multiplicative structure of the noise. The mere presence of non-Gaussianity, therefore, does not necessarily imply that the slow non-linearities are responsible for the non-Gaussian statistics.

Using a simple stochastic model provided by Monahan (2004), it has been shown that stochastically perturbing the drag coefficient of the momentum equations for a turbulent boundary layer is consistent with data. That is, perturbing the drag coefficient is not just an ad hoc way to introduce noise into models, but is a physically consistent approach to stochastically parameterize subgrid scale processes; the turbulent nature of the subgrid scale processes is sufficiently disordered as to make the the application of the Central Limit Theorem valid (e.g., Khasminskii 1966; Papanicolaou and Kohler 1974; Majda et al. 1999, 2003). In particular, the velocity decorrelation times in the boundary layer are short enough to make the white-noise approximation valid.

The implications of the presented results are at least twofold. First, the potentially significant role of stochastic parameterizations in climate models has been stressed in several studies (e.g., Buizza et al. 1999; Palmer 2001; Sardeshmukh et al. 2001; Pérez-Muñuzuri et al. 2003; Sura 2002; Sura et al. 2004). Here, it has been shown that perturbing the damping parameters is a physically consistent step towards stochastic parameterizations in complex climate models. Second, it has been shown by Sura and Penland (2002) and Sura and Gille

(2003) that the detailed knowledge of wind statistics are vital to understand and model oceanic variability: the accuracy of a stochastic model crucially depends on how appropriate the stochastic representation is to the physical process it is meant to represent.

In summary, a comprehensive approach towards a better understanding of atmospheric variability, and its subsequent impact on oceanic variability, must consider stochastic parameterizations and, therefore, state-dependent noise.

Acknowledgments.

We would like to thank Matt Newman and Cécile Penland for helpful discussions about stochastic dynamical systems. This work was funded by the Predictability DRI of the Office of Naval Research, Grant N00014-99-1-0021.

References

Bourassa, M. A., M. H. Freilich, D. M. Legler, W. T. Liu, and J. J. O'Brien, 1997: Wind observations from new satellite and research vessels agree, *EOS Trans. of Amer. Geophys. Union*, **78**, 597, 602.

Buizza, R., M. J. Miller, and T. N. Palmer, 1999: Stochastic simulation of model uncertainties in the ECMWF ensemble prediction system, *Quart. J. R. Met. Soc.*, **125**, 2887–2908.

Chin, T. M., R. F. Milliff, and W. G. Large, 1998: Basin-scale, high-wavenumber sea surface wind fields from a multiresolution analyses of scatterometer data, *J. Atmos. Oceanic Technol.*, **15**, 741–763.

Friedrich, R., and J. Peinke, 1997a: Description of a turbulent cascade by a Fokker-Planck equation, *Phys. Rev. Lett.*, **78**, 863–866.

Friedrich, R., and J. Peinke, 1997b: Statistical properties of a turbulent cascade, *Physica D*, **102**, 147–155.

Friedrich, R., C. Renner, M. Siefert, and J. Peinke, 2002: Comment on "Indispensable finite time corrections for Fokker-Planck equations from time series data", *Phys. Rev. Lett.*, **89**, 149401(1).

Friedrich, R., S. Siegert, J. Peinke, S. Lück, M. Siefert, M. Lindemann, J. Raethjen, G. Deusch, and G. Pfister, 2000: Extracting model equations from experimental data, *Phys. Lett. A*, **271**, 217–222.

Gardiner, C. W., 1985: *Handbook of Stochastic Methods for Physics, Chemistry and the Natural Science, Second Edition*, Springer-Verlag, 442 pp.

Gille, S. T., 2003: Statistical characterization of ocean vector winds, *J. Atmos. Sci.*, submitted.

Gradišek, J., S. Siegert, R. Friedrich, and I. Grabec, 2000: Analysis of time series from stochastic processes, *Phys. Rev. E*, **62**, 3146–3155.

Haltiner, G. J., and R. T. Williams, 1980: *Numerical Weather Prediction and Dynamic Meteorology*, Wiley, New York, 477 pp.

Hasselmann, K., 1976: Stochastic climate models. Part I. Theory, *Tellus*, **28**, 473–484.

Horsthemke, W., and R. Léfèver, 1984: *Noise-Induced Transitions: Theory and Applications in Physics, Chemistry, and Biology*, Springer-Verlag, 318 pp.

Imkeller, P., and J.-S. von Storch, eds., 2001: *Stochastic Climate Models*, vol. 49 of *Progress in Probability*, Birkhäuser Verlag, 398 pp.

Khasminskii, R. Z., 1966: A limit theorem for the solutions of differential equations woth random right hand side, *Theor. Prob. Appl*, **11**, 390–406.

Kimoto, M., and M. Ghil, 1993: Multiple flow regimes in the northern hemisphere winter. Part I: Methodology and hemispheric regimes, *J. Atmos. Sci.*, **50**, 2625–2643.

Majda, A. J., I. Timofeyev, and E. Vanden Eijnden, 1999: Models for stochastic climate prediction, *PNAS*, **96**, 14687–14691.

Majda, A. J., I. Timofeyev, and E. Vanden Eijnden, 2003: Systematic strategies for stochastic mode reduction in climate, *J. Atmos. Sci.*, **60**, 1705–1722.

Milliff, R. F., W. G. Large, J. Morzel, and G. Danabasoglu, 1999: Ocean general circulation model sensitivity to forcing from scatterometer winds, *J. Geophys. Res., Oceans*, **104**, 11337–11358.

Monahan, A. H., 2004: A simple model for the skewness of global sea-surface winds, *J. Atmos. Sci.*, **61**, 2037–2049.

Palmer, T. N., 2001: A nonlinear dynamical perspective on model error: A proposal for non-local stochastic-dynamic parametrization in weather and climate prediction models, *Quart. J. R. Met. Soc.*, **127**, 279–304.

Papanicolaou, G., and W. Kohler, 1974: Asymptotic theory of mmxing stochastic differential equations, *Commun. Pure Appl. Math*, **96**, 641–668.

Patoux, J., and R. A. Brown, 2001: Spectral analysis of QuikSCAT surface winds and two-dimensional turbulence, *J. Geophys. Res., Atmospheres*, **106**, 23995–24005.

Paul, W., and J. Baschnagel, 1999: *Stochastic Processes: From Physics to Finance*, Springer-Verlag, 231 pp.

Penland, C., 1996: A stochastic model of Indio Pacific sea surface temperature anomalies, *Phys. D*, **98**, 543–558.

Penland, C., 2003a: Noise out of chaos and why it won't go away, *Bulletin of the American Meteorological Society*, **84**, 921–925.

Penland, C., 2003b: A stochastic approach to nonlinear dynamics: A review (electonic supplement to 'noise out of chaos and why it won't go away'), *Bulletin of the American Meteorological Society*, **84**, ES43–ES51.

Pérez-Muñuzuri, V., M. N. Lorenzo, P. Montero, K. Fraedrich, E. Kirk, and F. Lunkeit, 2003: Response of a global atmospheric circulation model to spatio-temporal stochastic forcing: Ensemble statistics, *Nonlinear Processes Geophys.*, **10**, 453–461.

Ragwitz, M., and H. Kantz, 2001: Indispensable finite time corrections for Fokker-Planck equations from time series data, *Phys. Rev. Lett.*, **87**, 254501(1)–254501(4).

Renner, C., J. Peinke, and R. Friedrich, 2001: Experimental indications of Markov properties of small-scale turbulence, *J. Fluid Mech.*, **433**, 383–409.

Sardeshmukh, P., C. Penland, and M. Newman, 2001: Rossby waves in a fluctuating medium, *Progress in Probability, Vol. 49: Stochastic Climate Models*, P. Imkeller, and J.-S. von Storch, eds., Birkhäuser Verlag, Basel.

Siegert, S., R. Friedrich, and J. Peinke, 1998: Analysis of data sets of stochastic systems, *Phys. Lett. A*, **243**, 275–280.

Sura, P., 2002: Noise induced transitions in a barotropic β-plane channel, *J. Atmos. Sci.*, **59**, 97–110.

Sura, P., 2003: Stochastic analysis of Southern and Pacific Ocean sea surface winds, *J. Atmos. Sci.*, **60**, 654–666.

Sura, P., and J. J. Barsugli, 2002: A note on estimating drift and diffusion parameters from timeseries, *Phys. Lett. A*, **305**, 304–311.

Sura, P., and S. T. Gille, 2003: Interpreting wind-driven Southern Ocean variability in a stochastic framework, *Journal of Marine Research*, **61**, 313–334.

Sura, P., M. Newman, C. Penland, and P. D. Sardeshmukh, 2004: Multiplicative noise and non-Gaussianity: A paradigm for atmospheric regimes?, *J. Atmos. Sci.*, in press.

Sura, P., and C. Penland, 2002: Sensitivity of a double-gyre ocean model to details of stochastic forcing, *Ocean Modelling*, **4**, 327–345.

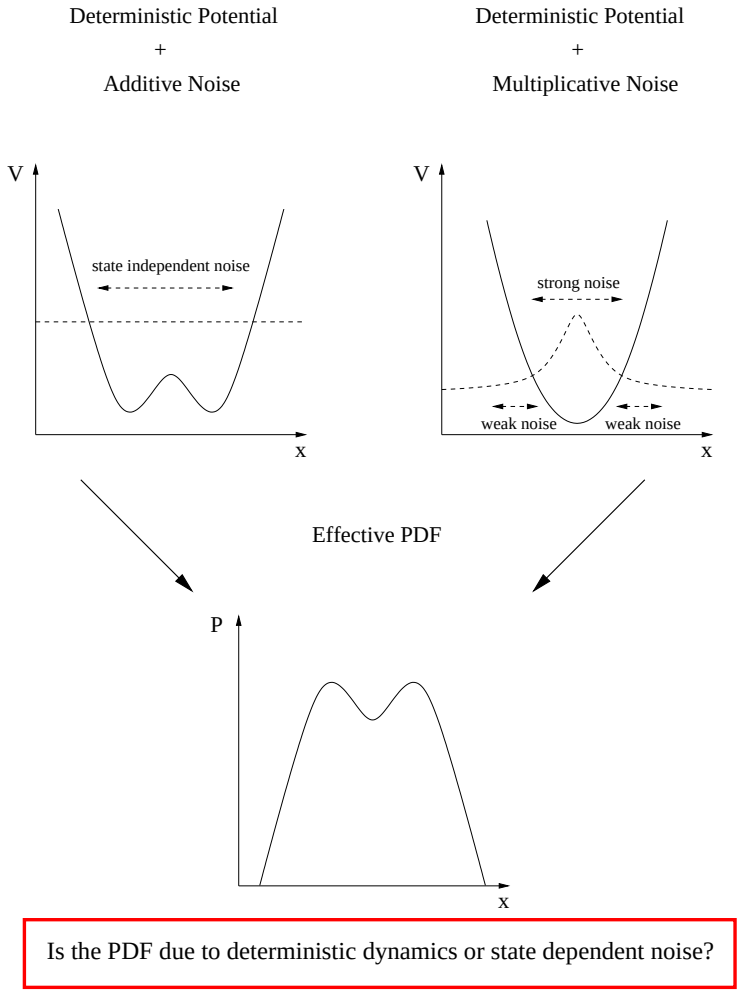

Figure 1: A schematic sketch to illustrate the fundamental dynamical difference between deterministically and stochastically induced regimes. The effective PDF of a trajectory in a deterministic double-well potential driven by additive noise will be bimodal. The same effective PDF can be produced by a trajectory in a monomodal deterministic potential kicked around by multiplicative noise. Because of the larger noise amplitudes near the center of the monomodal potential, as compared to the strength of the noise right and left from it, the system's trajectory is more often found on either side of the central noise maximum. Thus, the PDF becomes bimodal. See Sura et al. (2004) for a more detailed discussion of this behavior.

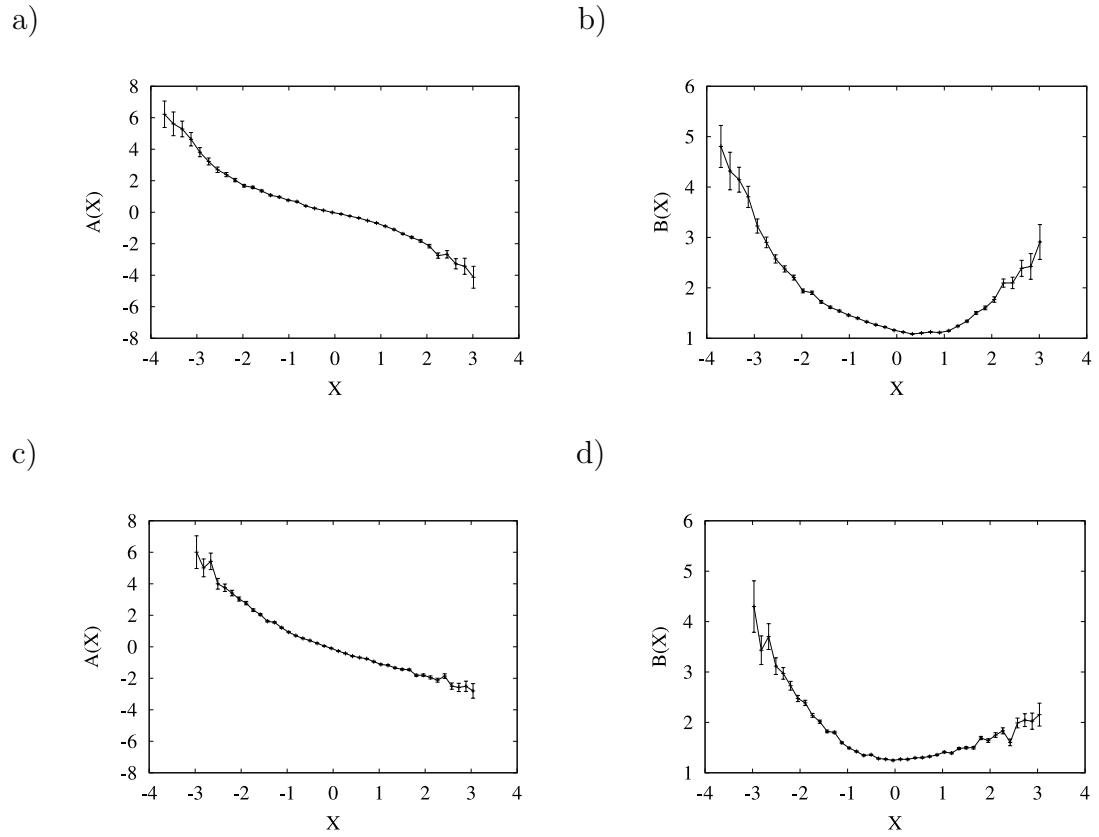

Figure 2: a) The estimated effective drift $A(x)$ and b) the estimated noise $B(x)$ for the zonal wind (u) at 50°S (Southern Ocean). c) The estimated effective drift $A(x)$ and d) the estimated noise $B(x)$ for the meridional wind (v) at 50°S (Southern Ocean). The error bars indicate one $\pm$ one standard error.

a)

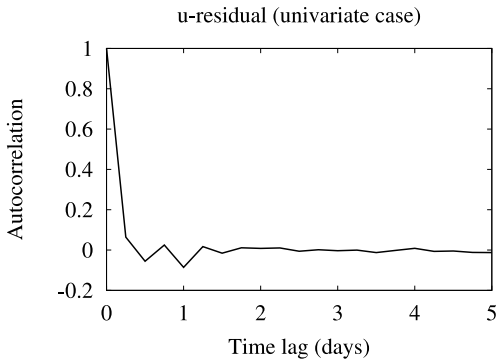

b)

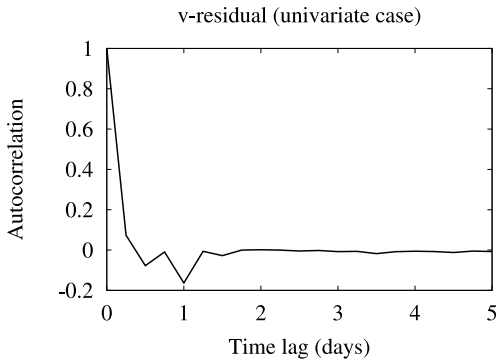

c)

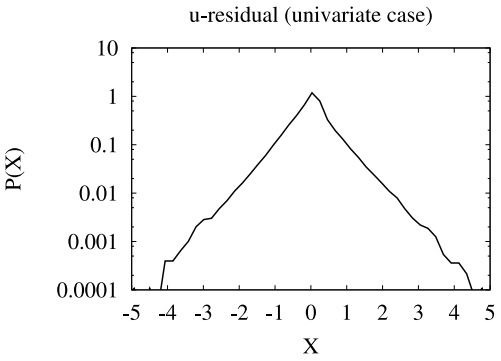

d)

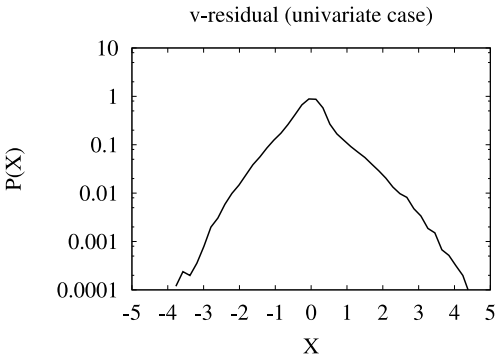

Figure 3: Autocorrelation functions (a,b) and PDFs (c,d) of the residuals $r \equiv x_{obs}(t+\Delta t) - x(t+\Delta t)$ for the univariate zonal (a,c) and meridional (b,d) winds. Note that for both the zonal and the meridional wind the autocorrelation is close to zero after one time step of 0.25 days, and that the residuals are highly non-Gaussian; see section 4.1 for details.

a)

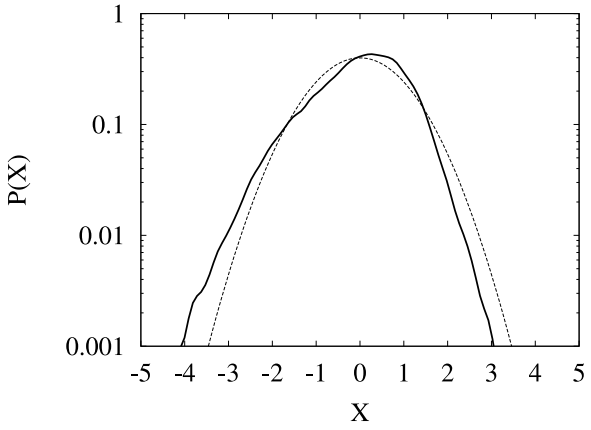

b)

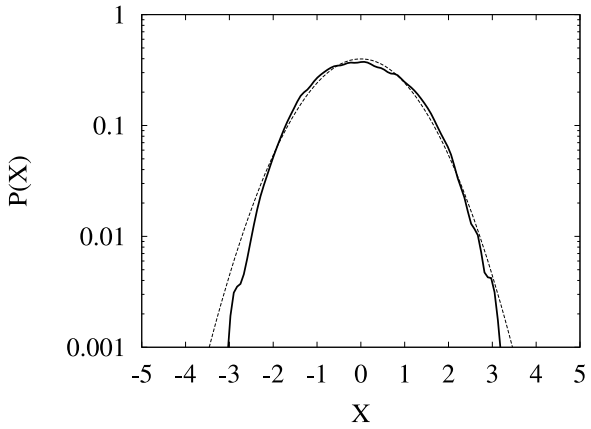

Figure 4: PDFs obtained from wind data (solid lines) and the corresponding Gaussian PDFs (dashed lines): a) for the zonal wind (u), and b) for the meridional wind (v) at 50°S (Southern Ocean).

a)

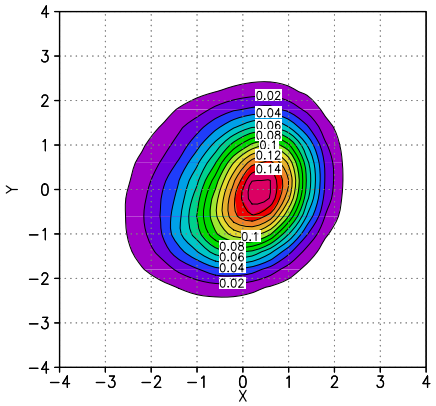

b)

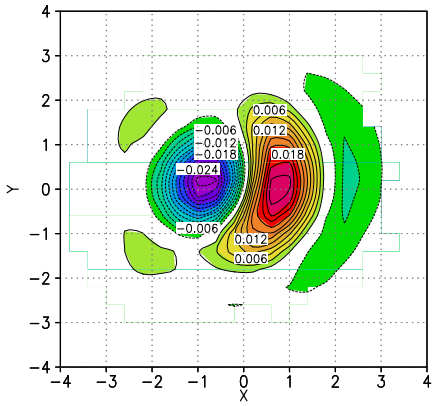

Figure 5: a) The joint PDF of the normalized zonal (u) and meridional wind (v) at 50°S (Southern Ocean). The contour interval is 0.01. b) The actual PDF anomalies of the normalized zonal (u) and meridional wind (v). The contour interval is 0.02. The deviations from a bivariate Gaussian PDF are significant at the 95% confidence level. In both figures the x-component represents the zonal wind (u), and the y-componen the meridional wind (v).

a)

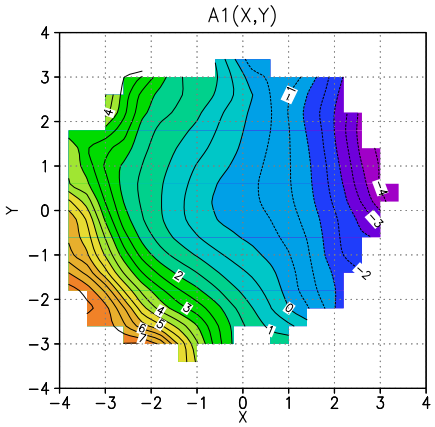

b)

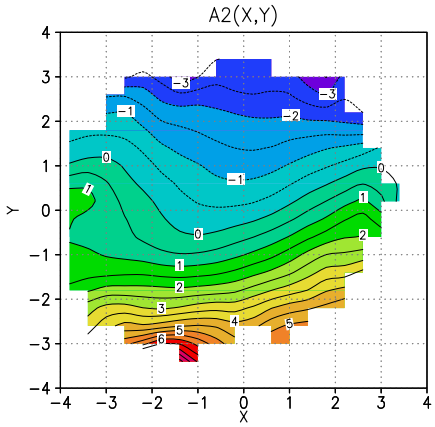

Figure 6: The effective drift $\mathbf{A}(\mathbf{x})$ estimated from wind vectors at 50°S (Southern Ocean). a) $A1(x, y)$ denotes the x-component (zonal wind), and b) $A2(x, y)$ denotes the y-component (meridional wind) of the two-dimensional system. The contour interval is 0.5.

a)

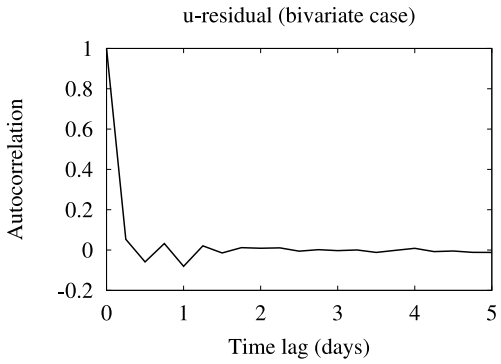

b)

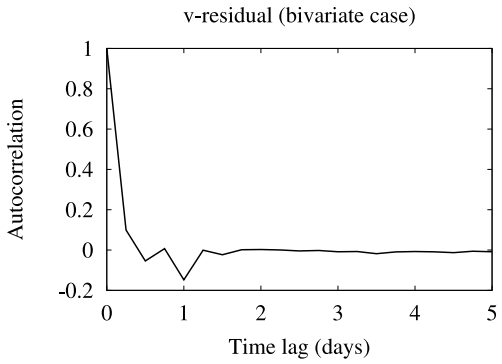

c)

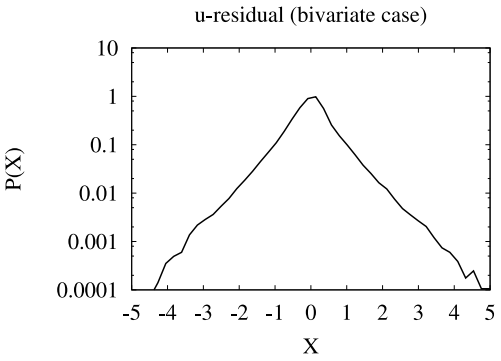

d)

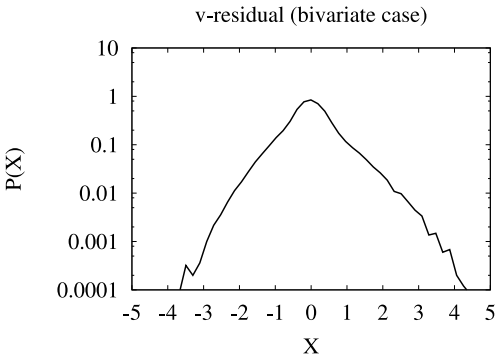

Figure 7: Autocorrelation functions (a,b) and PDFs (c,d) of the residuals $\mathbf{r} \equiv \mathbf{x}_{obs}(t+\Delta t) - \mathbf{x}(t+\Delta t)$ for the bivariate zonal (a,c) and meridional (b,d) winds. Note that for both the zonal and the meridional wind the autocorrelation is close to zero after one time step of 0.25 days, and that the residuals are highly non-Gaussian; see section 4.2 for details.

a) b)

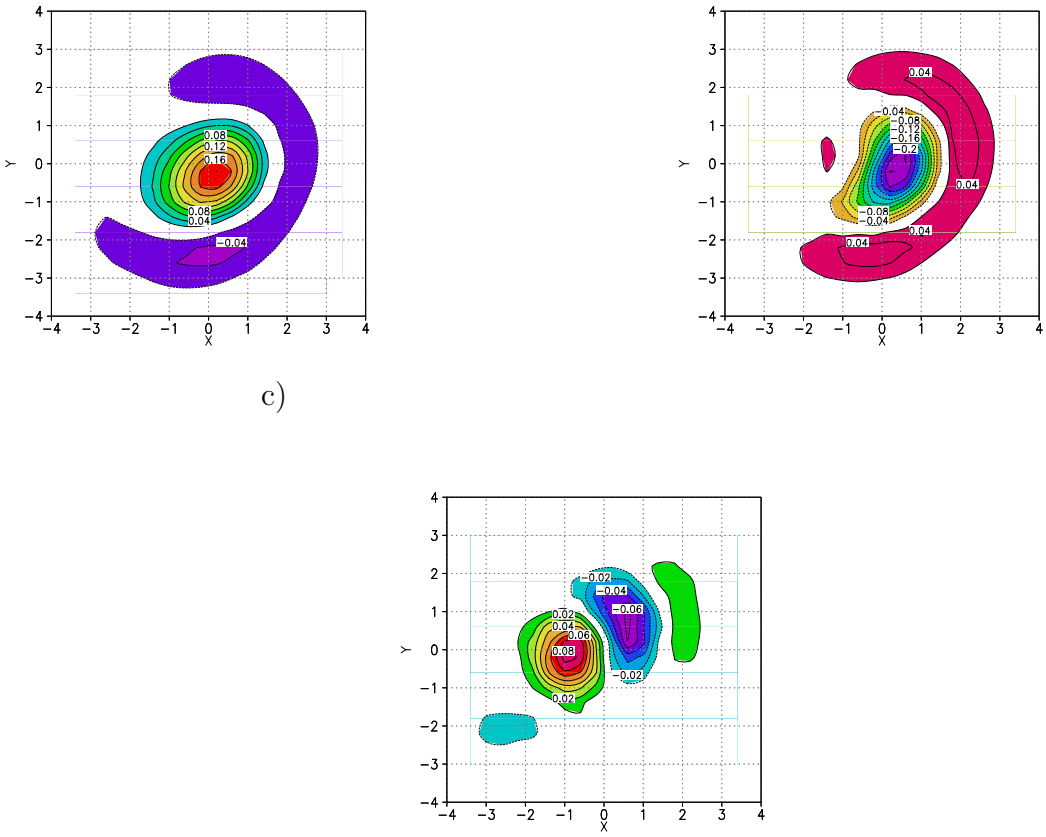

c)

Figure 8: a) The effective deterministic term, b) the stochastic term (the dark dashed line indicates the zero contour; see text for details), and c) the sum of the effective deterministic and the stochastic term of the steady Fokker-Planck equation (9) evaluated by using the PDF (Fig. 5), the deterministic drift (Fig. 6), and pure additive noise given by the matrix (10). The negative value of that sum ($-R$) can be interpreted as the multiplicative noise contribution of the Fokker-Planck equation (9); positive (negative) values mean that the additive noise is too weak (strong) to balance the deterministic term. The shown regions are significant at the 95% confidence level. The x-component represents the zonal wind (u), the y-component the meridional wind (v). In a) and b) the contour interval is 0.02, in c) it is 0.01.

a)

b)

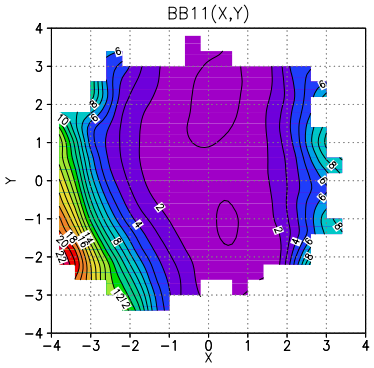

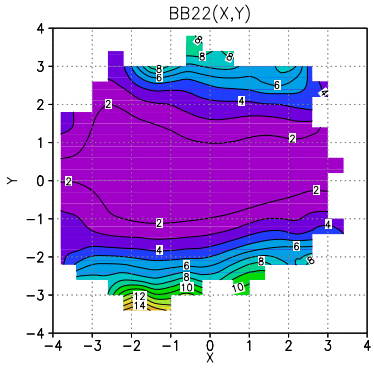

c)

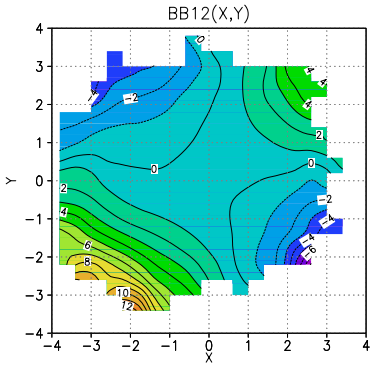

Figure 9: The elements of the matrix $\mathbf{B}(\mathbf{x})\mathbf{B}^T(\mathbf{x})$ directly estimated from wind vectors at 50°S (Southern Ocean): a) $(\mathbf{B}\mathbf{B}^T)_{11}$, b) $(\mathbf{B}\mathbf{B}^T)_{22}$, and c) $(\mathbf{B}\mathbf{B}^T)_{12}$. Note that $\mathbf{B}\mathbf{B}^T$ is symmetric: $(\mathbf{B}\mathbf{B}^T)_{12} = (\mathbf{B}\mathbf{B}^T)_{21}$. The x-component represents the zonal wind (u), the y-component the meridional wind (v). In all plots the contour interval is 1.

a)

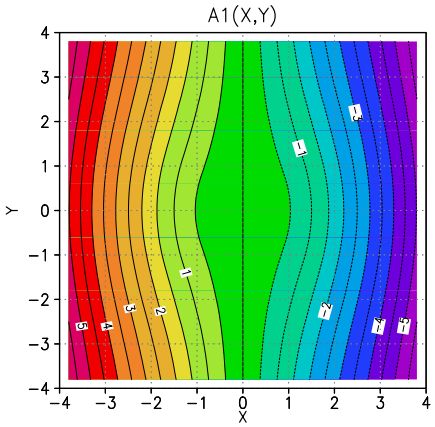

b)

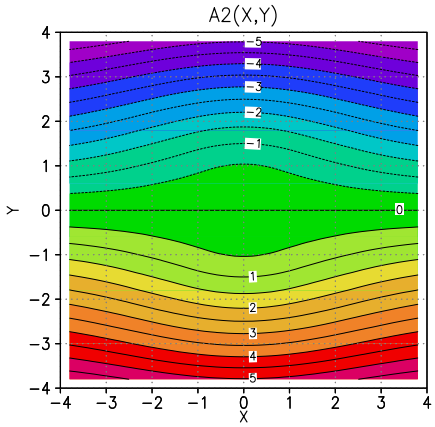

Figure 10: The theoretically derived function $\mathbf{A}(\mathbf{x})$ (Eq. 13). a) $A1(x, y)$ denotes the x-component (zonal wind), and b) $A2(x, y)$ denotes the y-component (meridional wind) of the two-dimensional system. In both plots the contour interval is 0.5.

a)

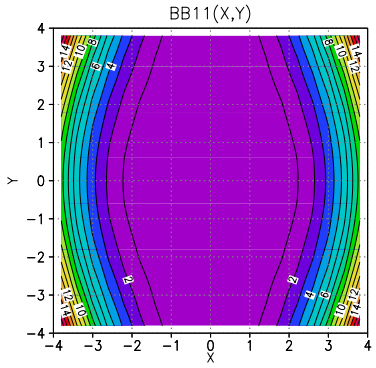

b)

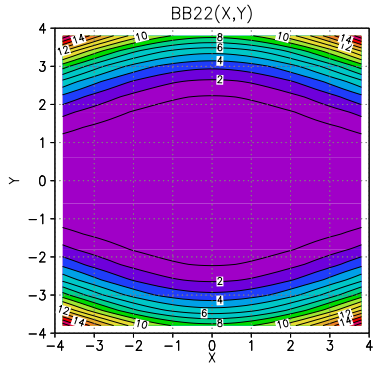

c)

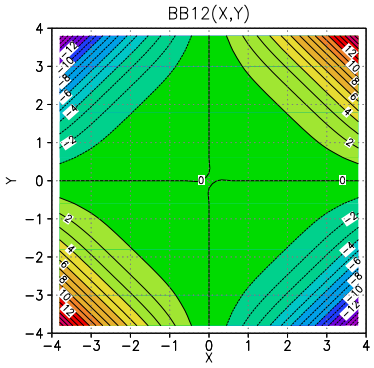

Figure 11: The theoretically derived elements of the matrix $\mathbf{B}(\mathbf{x})\mathbf{B}^T(\mathbf{x})$ (Eq. 15): a) $(\mathbf{B}\mathbf{B}^T)_{11}$, b) $(\mathbf{B}\mathbf{B}^T)_{22}$, and c) $(\mathbf{B}\mathbf{B}^T)_{12}$. The matrix is scaled to have the same order of magnitude as the matrix estimated from normalized wind data. Note that $\mathbf{B}\mathbf{B}^T$ is symmetric: $(\mathbf{B}\mathbf{B}^T)_{12} = (\mathbf{B}\mathbf{B}^T)_{21}$. In all plots the contour interval is 1.